Semiconductor nanocrystals in a magnetic field

J. Planelles, J. G. Díaz, and J. Climente
Departament de Ciències Experimentals, UJI, Castelló, Spain

W. Jaskólski
Instytut Fizyki UMK, Grudziądzka 5, 87-100 Toruń, Poland

(Received 9 January 2002; published 28 May 2002)

The influence of a magnetic field on the electron and hole energy spectra of spherical uniform and multilayer semiconductor nanocrystals is investigated. The calculations are performed within the $\mathbf{k}\cdot\mathbf{p}$ method and envelope function approximation. The valence subband mixing is taken into account by considering a two-band Hamiltonian for the hole states. It is shown that the magnetic-field dependence of the energy spectrum varies strongly with the size and composition of the nanocrystals. Several interesting phenomena, like spatial polar separation of the one-electron charge density in quantum dot–quantum well structures or crossover from confinement in the external shell to the internal core in quantum dot–quantum barrier systems under the influence of a magnetic field are reported.

DOI: 10.1103/PhysRevB.65.245302 PACS number(s): 73.21.La

I. INTRODUCTION

Semiconductor nanocrystals synthesized in colloidal solutions are the smallest quantum dots with the strongest three-dimensional confinement.[1–6] Their sizes can vary from 1 to 10 nm, they have frequently spherical shapes and can be fabricated as multishell structures, i.e., built of concentric layers (shells) of different semiconductors with the shell thickness down to a single monolayer. The size of the nanocrystals and the composition of layers can be easily manipulated in the process of fabrication, which makes it possible to tailor to a large extent their discrete energy spectra.[7,8] This makes them attractive for applications in novel optoelectronic devices.

The influence of a magnetic field on the energy structure of quantum dots has been studied so far almost exclusively for quasi-two-dimensional semiconductor islands, disks, and rings.[9–14] In the majority of works only electron states have been investigated and the calculations performed within the one-band effective-mass approximation with parabolic confining potentials. In such cases the resulting energy spectra are of the well-known Fock-Darwin type. However, when the effective-mass approach and the envelope function approximation are used, the confining potentials are far from being parabolic. They have a well defined steplike character at interfaces separating two different media: the rectangular steps are determined by the corresponding band offsets. Very recently, steplike potentials have been used to investigate and successfully explain[14] the energy spectra of InAs rings grown on GaAs substrate.[12,15] Such potentials have been also used in the study of resonance states of multilayer spherical nanocrystals, where an interesting phenomenon, the transformation of resonant states into bound states under the influence of a magnetic field, has been reported.[16,17]

In this paper we study the influence of a magnetic field on both the electron and hole energy levels of uniform and multishell spherical nanocrystals. The one-band effective-mass approach is used in the calculations of electron states. For the hole states the valence subband mixing is taken into account by considering a two-band Hamiltonian.[14,18] In multilayer structures, like quantum dot–quantum wells or quantum dot–quantum barriers, the charge density of some electron and hole states can be localized inside thin spherical layers.[7,8] We show that application of a magnetic field can lead in such structures to effects not observed for homogeneous spherical or two-dimensional quantum dots.

II. THEORY AND COMPUTATIONAL DETAILS

The one-band effective-mass equation for an electron in a spherical quantum dot potential $V_e(\rho,z)$ and magnetic field $\mathbf{B}=(0,0,B)$ is (in cylindrical coordinates ρ,z)

$$\left(\frac{1}{2m^*}\Delta-\frac{B^2}{8m^*}\rho^2-\frac{BM}{2m^*}+V_e(\rho,z)-E_{n,M}\right)\Phi_{nM}=0, \tag{1}$$

where $M=0,\pm1,\pm2,\cdots$ is the quantum number of the projection of the angular momentum $\mathbf{L}$ onto the magnetic-field (B) axis, m^* is the effective mass, and n is the main quantum number. For comparison with the spherically symmetric states of the $B=0$ case, we will label the consecutive states by $\tilde{n}L_M$, where $\tilde{n}$ labels the consecutive states of a given spherical symmetry case at $B=0$.

For the proper description of the valence-band states, the valence-subband mixing has to be taken into account by considering at least the four-band $\mathbf{k}\cdot\mathbf{p}$ Hamiltonian, that couples the heavy hole and light hole subbands.[19] The four-band Hamiltonian represented in the conventional Luttinger-Kohn basis depends on two Luttinger parameters γ and γ_1, which determine the heavy-hole and light-hole effective masses $m_{hh}=1/(\gamma-2\gamma_1)$ and $m_{ll}=1/(\gamma+2\gamma_1)$. When zero-dimensional nanostructures are considered, in which the electrons and holes can be totally confined in three dimen-

sions, the envelope function approximation is applied and the elements of the Hamiltonian become the operators acting on the components f_i of the envelope function.

For spherical nanostructures, such as the ones investigated in this paper, the Hamiltonian is usually written in spherical coordinates and results in two coupled differential equations in the radial variable.[19] When the external magnetic field is applied the spherical symmetry is broken and the Hamiltonian commutes only with the operator $\mathbf{F}_z$ of the projection of the total angular momentum $\mathbf{F}=\mathbf{L}+\mathbf{J}$ onto the field axis ($\mathbf{J}$ is the Bloch angular momentum ($J=3/2$) and $\mathbf{L}$ is the envelope angular momentum). In such a case cylindrical coordinates (ρ,z,ϕ) are more convenient.[20] When the Hamiltonian is written down in cylindrical coordinates and integration over the ϕ angle is performed, it results in four coupled differential equations for the envelope function components (i) $f^i_{F_z}(\rho,z)$.[14]

The diagonal elements of the Hamiltonian include also (i) the potential energy $V_h(\rho,z)$, that depends on the actual geometry and structure of the studied system, and (ii) the interaction with an external uniform magnetic field $\mathbf{B}=(0,0,B)$ (linear Zeeman and quadratic terms). It is worthwhile to note that the cylindrical representation is also useful in the study of nonspherical nanocrystals (hemispherical, lens-shape, quantum rings,[14,12] two or more aligned and interacting nanocrystals[21]) or when additionally an external electric field is applied.

In looking for the bound states of the investigated systems all the envelope function components are required to vanish for large ρ and z. For multishell structures, V_h and V_e are formed by the valence-band and conduction-band offsets, respectively. Since the electron and hole effective masses are different in different layers, appropriate matching conditions should in general be applied at the corresponding interfaces. In this paper, for simplicity, uniform electron effective masses and Luttinger parameters are considered for all the investigated systems.

The electron [Eq. (1)] and hole[14] equations have been solved numerically using the finite-difference method on the two-dimensional grid (ρ,z) in cylindrical coordinates. The discretization of the differential equations yields eigenvalue problems of asymmetric huge and sparse matrices that have been solved by employing the iterative Arnoldi factorizations[22] implemented in the ARPACK package.[23]

III. RESULTS AND DISCUSSION

A. Uniform nanocrystals

1. Electron states

Chemically synthesized InAs nanocrystals are known of having almost spherical shapes.[2,24] Their typical sizes are 2–10 nm (in diameter). The particularly small electron effective mass of InAs, $m^*=0.024$, opens a possibility to study the magnetic-field effects in *artificial atoms*, that cannot be investigated in real atoms for the fields attainable in the laboratory. In this section we study the influence of a magnetic field on the electron energy structure of uniform InAs nanocrystals. We have performed the calculations for two nanocrystals of very different size, namely 6 and 23 nm in diameter, both surrounded by a 4-eV rectangular barrier modeling the vacuum, water solution, or polymer medium. The electron energy levels of the smaller nanocrystal versus magnetic

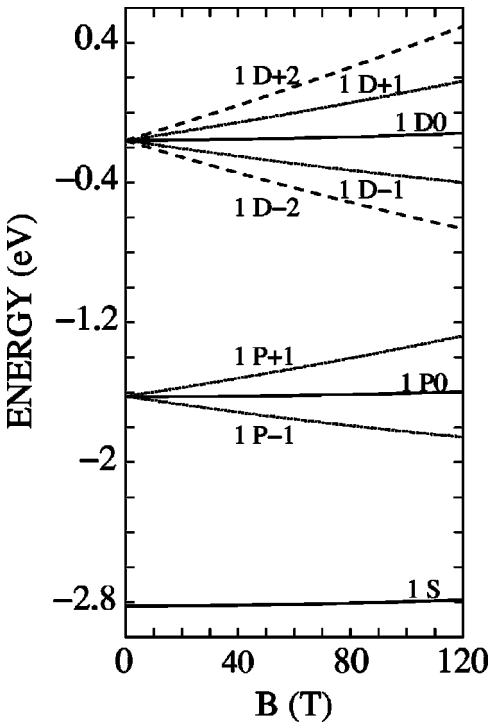

FIG. 1. Electron energy levels, $\tilde{n}LM$, for a uniform InAs nanocrystal of diameter $d=6$ nm vs magnetic field.

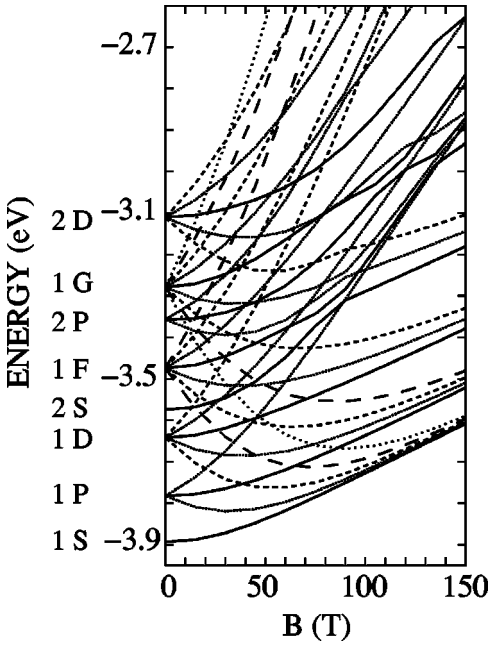

FIG. 2. Several lowest electron energy levels for a uniform InAs nanocrystal of diameter $d=23$ nm vs magnetic field. Degenerate $\tilde{n}$ levels for $B=0$ T are marked. $M=0$ solid lines, $M=\pm1$ dotted lines, $M=\pm2$ short dashed lines, $M=\pm3$ dashed lines.

field are presented in Fig. 1. Figure 2 shows the lower part of the energy spectrum of the wider quantum dot. The zero of energy scale is at the top of the external barrier.

For small nanocrystals the field dependence of the energy levels is, like in atoms, almost exclusively linear even for fields as strong as 100 T. In quantum dots of diameter $d \sim 10$ nm the quadratic dependence of the energy levels on the field starts to be seen at fields >70 T. In large nanocrystals, i.e., for $d>20$ nm, the quadratic dependence is seen already for laboratory fields (Fig. 2). The beginning of the formation of the first few Landau levels for fields greater than 100 T is also seen. For a very strong magnetic field the energy levels contributing to each Landau level form the spectrum of a one-dimensional rectangular potential well (in the z direction) of size d and depth 4 eV.

It is the ratio between ρ_0 and r_{max}, where $\rho_o=[(2|M|+1)(\hbar/eB)]^{1/2}$ is the radius of the maximum charge density in the lowest Landau level, and r_{max} is the maximum of the radial charge density in a given quantum dot state that decides whether only the linear Zeeman term or also the quadratic term in the Hamiltonian (1) are significant. For $B=100$ T, $\rho_o=2.4$ nm. In nanocrystals of diameter $d=6$ nm, $r_{max}\approx 1.5$ nm and *compression* of the radial charge density in the plane perpendicular to the field axis does not occur ($\rho_o>r_{max}$). In this case only the linear term is significant. However, in large dots, e.g., for $d=23$ nm, $r_{max}\approx 10$ nm and is much larger than ρ_o even for $B=10$ T. In this case the field confinement in the (x,y) plane is, for $B>10$ T, stronger than the quantum dot confinement and the quadratic term becomes important.

The states, which for $B=0$ have at least one radial node and thus significant charge density in the outer part of the nanocrystal, are more affected by the field than the nodeless states. This causes several anticrossings of the energy levels of a given symmetry M that can be observed for a larger nanocrystal at $B>70$ T.

2. Hole states

In this section we study the influence of a magnetic field on the valence-band energy structure of uniform InAs nanocrystals. Luttinger parameters, $\gamma_1=19.7$ and $\gamma=8.4$, corresponding to heavy hole and light hole effective masses $m_{hh}=0.345$, $m_{lh}=0.027$, are used.[25] When there is no magnetic field, the calculations are usually performed in spherical coordinates and the valence-band states are abelled by Q_F, where Q denotes the spectroscopic notation for the lowest value of L in the wave function.[18] When the magnetic field is on and the calculations are performed in cylindrical coordinates, the states are labeled by F_z. To identify these states by their spherical notation at $B=0$ we have performed, for $B=0$, two sets of calculations in both coordinates. This allows us to label the states in cylindrical coordinates as $\tilde{n}Q_F,F_z$, where $\tilde{n}$ is the main quantum number corresponding to a given spherical symmetry Q_F.

The valence-band energy levels for a InAs nanocrystal of diameter $d=6$ nm are shown in Fig. 3. The height of the external barrier is, like for electrons, 4 eV. Since even for

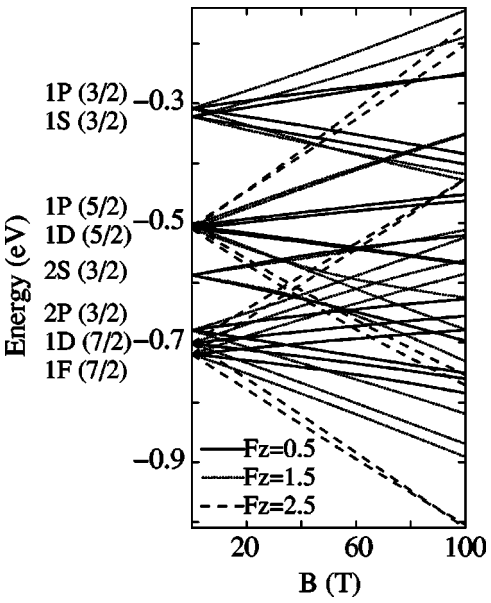

FIG. 3. Hole energy levels for a uniform InAs nanocrystal of diameter $d=6$ nm vs magnetic field. Degenerate $\tilde{n}Q(F)$ levels at $B=0$ T are marked.

$F_z=\frac{1}{2}$ the radius ρ_o of the maximum charge density in the corresponding Landau level is, for $B=100$ T, greater than 3 nm, the field dependence of the hole energy levels is for small nanocrystals again exclusively linear. One can see that the behavior of different pairs $\pm F_z$ of states of a given $|F_z|$ is different versus increasing magnetic field. For example, at $B=50$ T the energy difference $\Delta(1S_{\frac{3}{2}},+\frac{1}{2},1S_{\frac{3}{2}},-\frac{1}{2})$ is greater than $\Delta(1P_{\frac{5}{2}},+\frac{1}{2},1P_{\frac{5}{2}},-\frac{1}{2})$; the energy difference

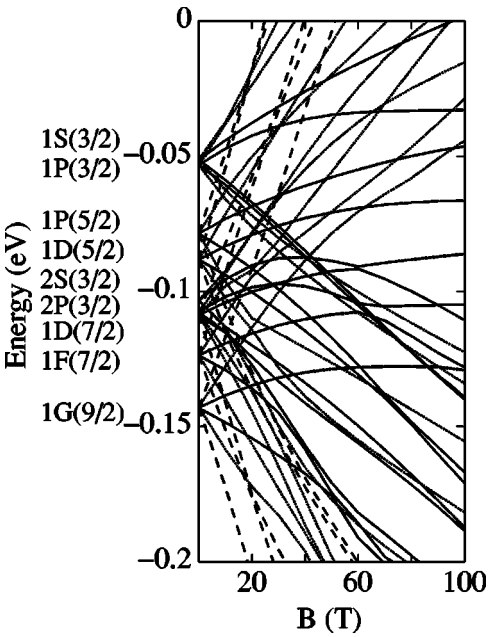

FIG. 4. Hole energy levels for a uniform InAs nanocrystal of diameter $d=16$ nm vs magnetic field. $F_z=\pm\frac{1}{2}$ solid lines, $F_z=\pm\frac{3}{2}$ dotted lines, $F_z=\pm\frac{5}{2}$ dashed lines. Degenerate $\tilde{n}Q(F)$ levels at $B=0$ T are marked.

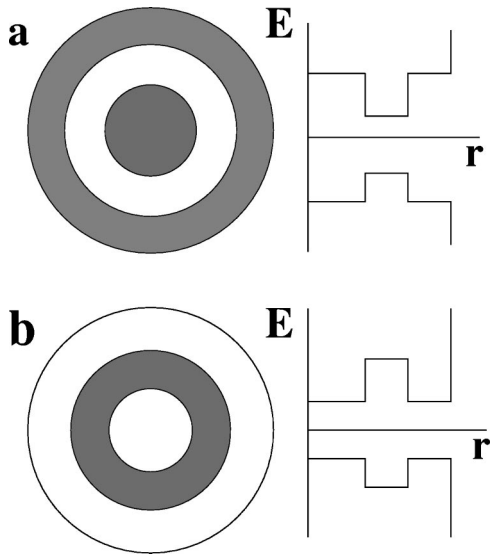

FIG. 5. The investigated multishell nanocrystals and the corresponding schematic layouts of conduction-band and valence-band edges. (a) quantum dot–quantum well, (b) quantum dot–quantum barrier.

$\Delta(1S_{\frac{3}{2}},+\frac{3}{2},1S_{\frac{3}{2}},-\frac{3}{2})$ is smaller than $\Delta(1P_{\frac{5}{2}},+\frac{3}{2},1P_{\frac{5}{2}},-\frac{3}{2})$. Another example: the energy difference $\Delta(2S_{\frac{3}{2}},+\frac{1}{2},2S_{\frac{3}{2}},-\frac{1}{2})$ is the same as $\Delta(2S_{\frac{3}{2}},+\frac{3}{2},2S_{\frac{3}{2}},-\frac{3}{2})$. This is because different pairs $\pm F_z$ of states correspond to two valence subbands of different effective masses resulting from mixed light and heavy hole subbands.

Figure 4 shows the energy levels versus magnetic field of a larger InAs nanocrystal of diameter $d=16$ nm. For the

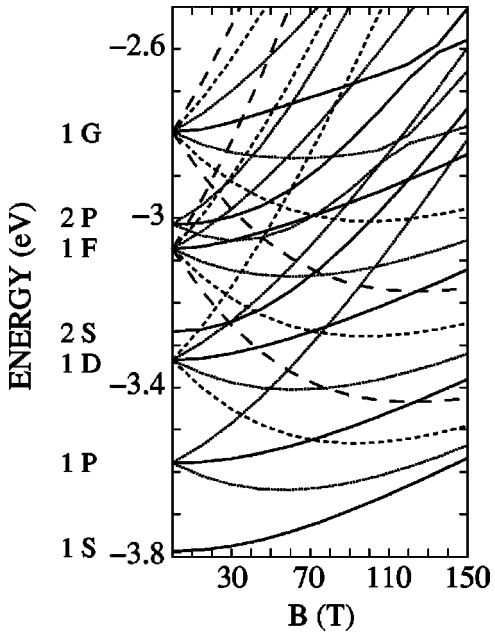

FIG. 6. Several lowest electron energy levels of a InAs(7 nm)/GaAs(1 nm)/InAs(2 nm) quantum dot–quantum barrier vs magnetic field. Degenerate $\tilde{n}L$ levels for $B=0$ T are marked. $M=0$ solid lines, $M=\pm1$ dotted lines, $M=\pm2$ short dashed lines, $M=\pm3$ dashed lines.

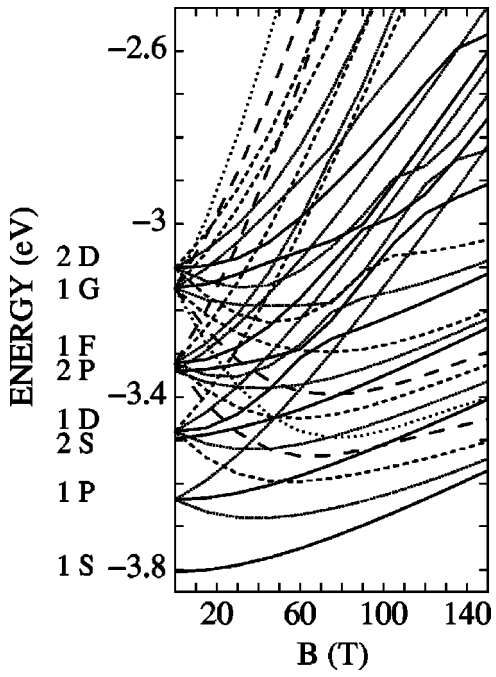

FIG. 7. The same as in Fig. 3, but for InAs(7 nm)/GaAs(1 nm)/InAs(3.5 nm).

states of $F_z=\pm\frac{1}{2}$ the quadratic term in the Hamiltonian now becomes significant even at laboratory fields, while for $F_z=\frac{5}{2}$ the linear term is still dominant, even at fields as strong as 50 T. The states of a given F_z, that for $B=0$ have a different number of nodes since they belong to different spherical symmetries, evolve in a different way versus increasing magnetic field. This causes several anticrossings well seen in Fig. 4. However, no anticrossings of F_z states belonging to the same spherical symmetry Q_F are seen, as is observed for semiconductor quantum rings.[14]

B. Quantum dot–quantum barrier

Let us consider a three-layer nanocrystal built of an internal InAs core of radius 7 nm, middle GaAs shell of thickness 1 nm, and external InAs clad. Since the forbidden energy gap of GaAs is wider than the gap of InAs, the middle shell acts for the conduction-band electrons as a 1-eV barrier separating two spherical InAs wells.[26] The surrounding medium is modeled by a 4-eV external potential barrier. The system and the corresponding band structure are shown schematically in Fig. 5(b).

The electron energy levels (versus magnetic field) of two nanostructures with an external InAs clad of thickness (a) 2 nm and (b) 3.5 nm are shown in Figs. 6 and 7. Only the states, which for $B=0$ have energies below the GaAs barrier, are shown (except for the $1G$ states of the smaller nanocrystal that have also been included in Fig. 3). Since the total diameters of these nanocrystals are 20 and 23 nm, respectively, the energy spectrum is similar to the spectrum of the uniform quantum dot studied in the previous section.

For $B=0$ a rearrangement of some energy levels ($1D$, $2S$) and ($1F$, $2P$) with the increasing thickness of the ex-

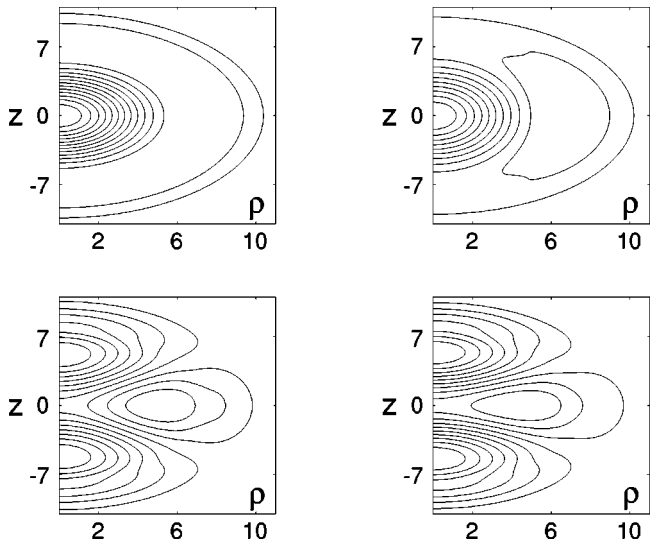

FIG. 8. InAs(7 nm)/GaAs(1 nm)/InAs(2 nm) quantum dot–quantum barrier. Charge-density contours of electron states $2S_0$ (top) and $1D_0$ (bottom) for $B=0$ T (left) and $B=40$ T (right). z and ρ in nm.

ternal shell, reported previously for CdS/ZnS/CdS nanocrystals,[7] is also observed here. Since the radial part of the $2S$ $(2P)$ state has a node, this state is favorable for building a significant charge density in the external clad in comparison to the nodeless $1D(1F)$ state. It causes faster decrease of the energy of the $2S(2P)$ state when the clad thickness increases.

On the other hand, since $1D_0$ and $1F_0$ states contribute to the lowest Landau level when the field is on, while $2S_0$ and $2P_0$ states contribute to second Landau level, more anticrossing points are observed for the wider-clad nanocrystal (Fig. 7). This is also illustrated in Figs. 8 and 9, where the contours of the charge densities of the $2S_0$ and $1D_0$ states

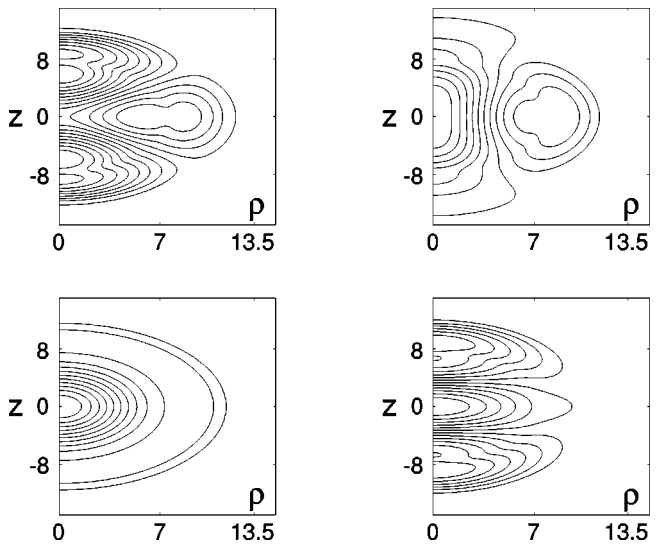

FIG. 9. The same as in Fig. 5, but for 3.5-nm external InAs clad. $B=0$ T (left) before $2S_0$ and $1D_0$ levels anticrossing; $B=40$ T (right) after anticrossing.

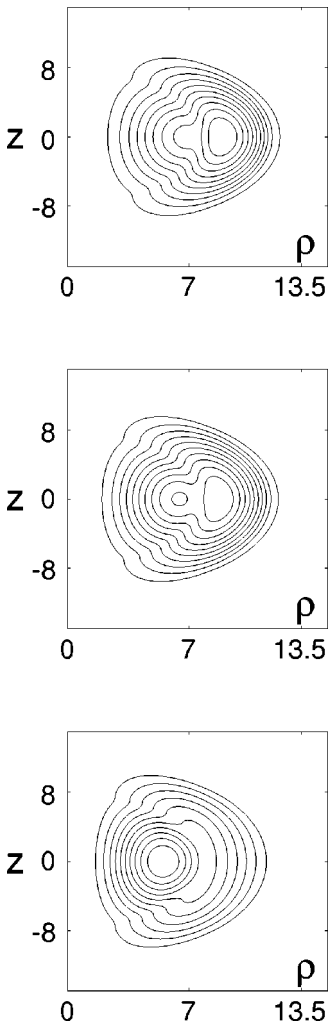

FIG. 10. Charge-density contours of $1F_3$ state of the larger quantum dot–quantum barrier system in a magnetic field $B=0$, $B=50$, and $B=100$ T (from top to bottom). z and ρ in nm. 1-nm wide GaAs barrier begins at $r=7$ nm.

for $B=0$ and $B=40$ T are shown for the cases with a thinner and thicker clad, respectively.

Some of the excited states can have, for $B=0$, the maximum of charge density localized in the external InAs clad. The $1F_3$ state (of the thicker nanocrystal) is one of the examples, in which the charge-density maximum is localized on a ring $(\rho_{ext}, z\approx 0)$, where ρ_{ext} is the radius of the external clad. A strong enough magnetic field can push the electron charge density from the external clad to the internal core. This is shown in Fig. 10. For nanocrystals with a larger core this can happen even for laboratory fields. This crossover from confinement in the external shell to confinement in the internal core can be used to modify the transition rates in the magneto-optical absorption spectra or binding strength of quantum dot molecules and quantum dot solids.[21]

C. Quantum dot–quantum well

Let us consider now a three-layer nanocrystal built of a internal barrier acting GaAs core, a middle well acting InAs

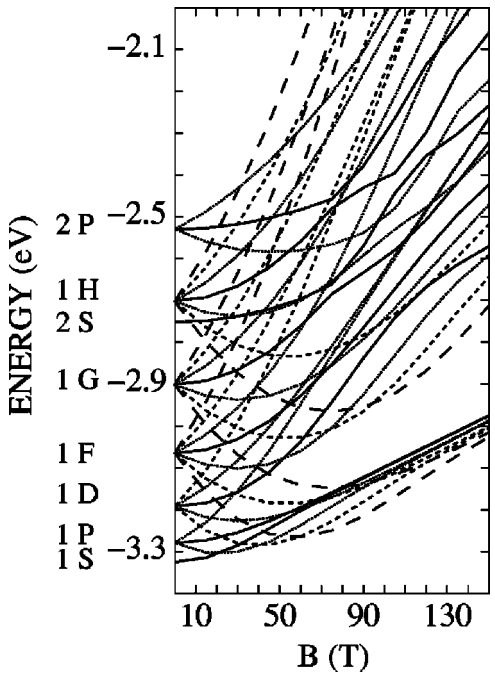

FIG. 11. Several electron energy levels for a GaAs(8 nm)/InAs(2 nm)/GaAs(2 nm) quantum dot–quantum well. Degenerate $\tilde{n}L$ levels for $B=0$ are marked. $M=0$ solid lines, $M=\pm 1$ dotted lines, $M=\pm 2$ short dashed lines, $M=\pm 3$ dashed lines.

shell, and an external barrier acting GaAs clad. The radius of the core is 8 nm, the thickness of the InAs and GaAs shells is 2 nm, and the height of the surrounding barrier is 4 eV (from the bottom of the InAs well). The system is schematically shown in Fig. 5(a). The electron energy levels versus magnetic field are shown in Fig. 11.

Although the energy spectrum looks, at first sight, similar to the ones of the uniform and quantum dot–quantum barrier structures, it differs in the change of the ground state symmetry with the increase of the magnetic field. Thus for $B<20$ T the ground state is $1S_0$, for $20<B<40$ T it is a $1P_{-1}$ state, for $40<B<60$ T it is $1D_{-2}$, next $1F_{-3}$, etc. This behavior is similar to the one observed in two-dimensional quantum rings.[12,14] In both cases, the wave function of the first state of each symmetry F_z (or M) has most of the electron charge density localized in the well (or ring). Therefore all such states have similar expectation value of $\langle \rho^2 \rangle$ and thus similar quadratic behavior in a magnetic field. Since at $B=0$ the corresponding energy levels are close, the linear term in the Hamiltonian causes the progressive change of the ground state versus increasing magnetic field.

Another interesting feature of this spectrum is that the first two energy levels of each symmetry approach each other as the magnetic field increases, so that they become almost degenerate at high fields. One can see it for $(1S_0,\ 1P_0)$, $(1P_{-1},\ 1D_{-1})$, $(1D_{-2},\ 1F_{-2})$, $(1P_{+1},\ 1D_{+1})$ and $(1D_{+1},\ 1F_{+1})$ pairs. Moreover, for very high fields, all the

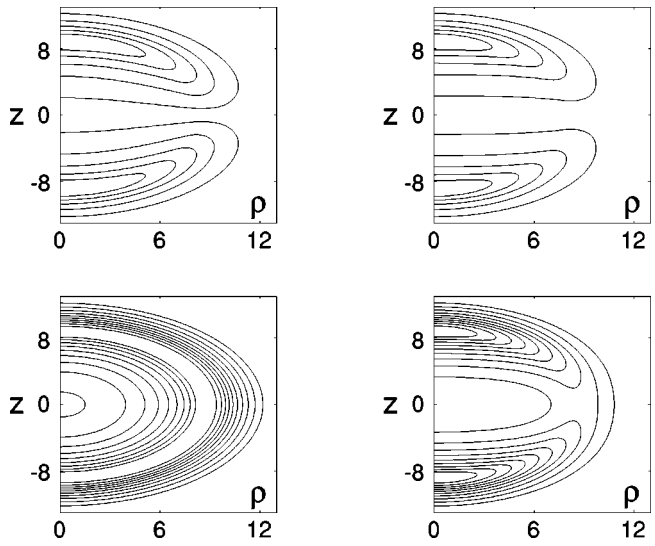

FIG. 12. Quantum dot–quantum well. Charge-density contours of electron state $1P_0$ (top) and $1S_0$ (bottom) for $B=0$ T (left) and $B=100$ T (right). z and ρ in nm.

energy levels contributing to the lowest Landau level group into a single level bound below the GaAs barrier. To explain these effects the contours of charge densities for the pair of states $(1S_0,\ 1P_0)$ at $B=0$ and $B=100$ T are plotted in Fig. 12.

The $1P_0$ state has, for $B=0$, a symmetry similar to a p_z atomic orbital. The increasing magnetic field tries to *squeeze* the charge into the small Landau orbit, but since it bounces the wide internal GaAs barrier, the charge concentrates finally in two spots, at which the z axis crosses the well acting InAs sphere. The same happens to the $1S_0$ state with the only difference that the wave function of the $1S_0$ state has the same sign in all the space, while the $1P_0$ state has a nodal plane at $z=0$.

In a very strong magnetic field the Landau states are *squeezed* so much that only confinement in the z direction survives from the initial three-dimensional (3D) confinement in the quantum dot. The resulting confining potential becomes almost one-dimensional with two narrow (2-nm wide) wells (1 eV deep) separated by a wide 16-nm barrier and $(1S_0,\ 1P_0)$ states being the *even* and *odd* solutions of such a double 1D well. Since the 1D well is very narrow, only a single bound state exists below the GaAs barrier edge (see Fig. 11). This transformation of one-electron states from uniform charge distribution to a distribution of one-electron charge on two spatially separated regions may appear interesting for quantum computing applications.

ACKNOWLEDGMENTS

Financial support from MSC Fund II, KBN-8T11B06218, DGESIC-MEC P1B97-0397, and UJI-Bancaixa-P1B97-23 is acknowledged. J.G.D. thanks Generalitat Valenciana and J.C. thanks MEC for the financial support.

[1] A. Mews, A. Eychmüller, M. Giersig, D. Schoos, and H. Weller, J. Phys. Chem. **98**, 934 (1994).
[2] A. P. Alivistatos, Nature (London) **271**, 933 (1996).
[3] A. Mews, A. V. Kadavanich, U. Banin, and A. P. Alivisatos, Phys. Rev. B **53**, R13 242 (1996).
[4] R. B. Little, M. A. El-Sayed, G. W. Bryant, and S. Burke, J. Chem. Phys. **114**, 1813 (2001).
[5] D. Norris and M. G. Bawendi, Phys. Rev. B **53**, 16 338 (1996).
[6] J. Lumin. **70**, 1 (1996) (Special Issue on Spectroscopy of Isolated and Assembled Semiconductor Nanocrystals).
[7] W. Jaskólski and G. W. Bryant, in *Optical Properties of Semiconductor Nanostructures*, edited by M. L. Sadowski, M. Potemski, and M. Grynberg, NATO Science Series 3, Vol. 81 (Kluver Academic Publishers, Dordrecht, 2000).
[8] G. W. Bryant and W. Jaskólski, Phys. Status Solidi B **224**, 751 (2001).
[9] L. Jacak, P. Hawrylak, and A. Wójs, *Quantum Dots* (Springer, Berlin, 1998).
[10] T. Chakraborty, *Quantum Dots* (Elsevier, Amsterdam, 1999).
[11] R. C. Ashoori, Nature (London) **379**, 413 (1996).
[12] A. Lorke, R. J. Luyken, A. O. Govorov, J. P. Kotthaus, J. M. Garcia, and P. M. Petroff, Phys. Rev. Lett. **84**, 2223 (2000).
[13] Z. Barticevic, M. Pacheco, and A. Latgé, Phys. Rev. B **62**, 6963 (2000).
[14] J. Planelles, W. Jaskólski, and I. Aliaga, Phys. Rev. B **65**, 033306 (2001).
[15] A. Emperador, M. Pi, M. Barranco, and A. Lorke, Phys. Rev. B **62**, 4573 (2000).
[16] M. Bylicki and W. Jaskólski, Phys. Rev. B **60**, 15 924 (1999).
[17] W. Jaskólski, M. Bosek, M. Bylicki, and J. Planelles, Vacuum **63**, 185 (2001).
[18] A. Baldereschi and N. O. Lipari, Phys. Rev. B **8**, 2697 (1973); G. B. Gregorian, E. M. Kazaryan, Al. L. Efros, and T. V. Yazeva, Sov. Phys. Solid State **32**, 1031 (1990); Al. L. Efros and M. Rosen, Phys. Rev. B **58**, 7120 (1998).
[19] P. C. Sercel and K. J. Vahala, Phys. Rev. B **42**, 3690 (1990).
[20] For $B \neq 0$, the axial approximation could be used instead of the spherical approximation, but for a more adequate comparison with the results obtained for $B = 0$, the spherical approximation is employed in all the cases.
[21] W. Jaskólski, G. W. Bryant, J. Planelles, and M. Zieliński, Int. J. Quantum Chem. (to be published).
[22] W. E. Arnoldi, Q. Appl. Math. **9**, 17 (1951); Y. Saad, *Numerical Methods for Large Scale Eigenvalue Problems* (Halsted Press, New York, 1992); R. B. Morgan, Math. Comput. **65**, 1213 (1996).
[23] R. B. Lehoucq, D. C. Sorensen, P. A. Vu, and C. Yang, ARPACK: Fortran subroutines for solving large scale eigenvalue problems, Release 2.1; R. B. Lehoucq, D. C. Sorensen, and C. Yang, *ARPACK User's Guide: Solution of Large-Scale Eigenvalue Problems with Implicit Restarted Arnoldi Methods* (SIAM, Philadelphia, 1998).
[24] U. Banin, C. J. Lee, A. A. Guzelian, A. V. Kadavanich, A. P. Alivisatos, W. Jaskólski, G. W. Bryant, Al. L. Efros, and M. Rosen, J. Chem. Phys. **109**, 2306 (1998).
[25] *Numerical Data and Functional Relationships in Science and Technology*, edited by O. Madelung, Landolt-Börnstein, New Series, Group III (Springer-Verlag, Berlin, 1982), Vol. 17.
[26] Y. W. Cao and U. Banin, J. Am. Chem. Soc. **122**, 9692 (2000).